Available online at www.sciencedirect.com
SCIENCE DIRECT®
International Journal of Solids and Structures 42 (2005) 103–122
INTERNATIONAL JOURNAL OF SOLIDS and STRUCTURES
www.elsevier.com/locate/ijsolstr

A generalized approach to formulate the consistent tangent stiffness in plasticity with application to the GLD porous material model

Jinkook Kim, Xiaosheng Gao *

Department of Mechanical Engineering, The University of Akron, Akron, OH 44325, USA

Received 4 February 2004; received in revised form 15 July 2004
Available online 8 September 2004

Abstract

It has been shown that the use of the consistent tangent moduli is crucial for preserving the quadratic convergence rate of the global Newton iterations in the solution of the incremental problem. In this paper, we present a general method to formulate the consistent tangent stiffness for plasticity. The robustness and efficiency of the proposed approach are examined by applying it to the isotropic material with J_2 flow plasticity and comparing the performance and the analysis results with the original implementation in the commercial finite element program ABAQUS. The proposed approach is then applied to an anisotropic porous plasticity model, the Gologanu–Leblond–Devaux model. Performance comparison between the consistent tangent stiffness and the conventional continuum tangent stiffness demonstrates significant improvement in convergence characteristics of the overall Newton iterations caused by using the consistent tangent matrix.

Keywords: Implicit finite element method; Backward Euler method; Consistent tangent moduli; Anisotropic plasticity; The Gologanu–Leblond–Devaux model; Ductile fracture

1. Introduction

Most previous research on computational plasticity has been focused on isotropic materials. Significant progresses have been made in development of algorithms to integrate the elastoplastic constitutive equations for J_2 flow plasticity and other material models where the flow potential can be expressed as a

* Corresponding author. Tel.: +1 330 972 2415; fax: +1 330 972 6027.
E-mail address: xgao@uakron.edu (X. Gao).

0020-7683/$ - see front matter
doi:10.1016/j.ijsolstr.2004.07.011

function of the stress invariants. The integration algorithm enables one to treat the elastoplastic problem over a typical time step as an equivalent elastic problem. Thus choice of the integration scheme is important for the accuracy and stability of the solution. Ortiz and PoPov (1985) carried out a systematic investigation of the accuracy and stability of the generalized trapezoidal and midpoint rules. Their studies show that for strain increments, which are several times of the size of the yield surface in strain space, the backward Euler method provides a stable and accurate integration algorithm. For the implicit finite element method, the equilibrium equations are written at the end of each increment. If a full Newton–Raphson scheme is used to solve these non-linear equations, the so-called 'tangent moduli' are needed. Simo and Taylor (1985) showed that the consistency between the tangent (stiffness) operator and the integration algorithm employed in the solution of incremental problem plays a crucial role in the preserving the quadratic convergence rate of the global Newton iterations. They derived a tangent stiffness matrix for the J_2 material that is fully consistent with the backward Euler integration algorithm. Aravas (1987), Lee and Zhang (1991), Zhang (1995) and Muhlich and Brocks (2003) conducted detailed studies of the backward Euler method for numerical integration of a class of pressure-dependent plasticity laws and obtained the tangent moduli by consistent linearization of the elastoplastic constitutive equations.

In recent years, the finite element method has been successfully applied to develop mechanism-based approaches for predicting failure of ductile materials. The most widely used continuum damage model for analyzing ductile fracture phenomena is due to Gurson (1977) with the modification by Tvergaard (1982). The Gurson–Tvergaard (GT) model is an example of the class of pressure-dependent plasticity laws considered by Aravas (1987) and Lee and Zhang (1991), which provides a constitutive relation for ductile solids containing spherical voids. The flow potential of the GT model depends on the first and second stress invariants as well as an additional internal variable, the void volume fraction. When the void volume fraction becomes zero, the GT model reduces to the J_2 flow plasticity. Computational approaches based on the GT model have successfully predicted the behavior of ductile crack growth under a variety of conditions, e.g., Needleman and Tvergaard (1987), Xia et al. (1995), Ruggieri et al. (1998), and Gao et al. (1998a,b). However, a distinct limitation of the GT model is the assumption that voids are spherical in materials. But many processed materials, such as rolled plates, have non-spherical voids. And even for materials having initially spherical voids, the voids will change to prolate or oblate shape after deformation, depending on the state of the applied stress. In order to overcome the limitations of the GT model, Gologanu et al. (1993, 1994, 1995) derived a yield function for materials containing spheroidal voids. During plastic deformation, both the volume fraction and the shape of voids evolve as deformation increases. Since non-spherical voids are considered in the constitutive model, preferred material orientation exists and the plastic behavior becomes anisotropic. Unlike the isotropic materials, which have no preferred material orientations so that the yield functions can be described by the stress invariants, the Gologanu–Leblond–Devaux (GLD) material has preferred orientation and exhibits anisotropic plastic behavior. Consequently the yield function of the GLD model is expressed in a complicated form in terms of the stress components. Recently Pardoen and Hutchinson (2000, 2003) implemented the GLD model in the finite element analysis and their results show that the computational approach based on the GLD model provides a promising tool to simulate the ductile fracture process and to predict failure of engineering structures. Due to the complexity of the constitutive equations of the GLD model, they adopted the conventional continuum tangent stiffness in their finite element implementation. Such a procedure, however, results in loss of the quadratic rate of asymptotic convergence particularly important for large time steps. Fracture analysis often deals with large finite element models and requires efficient numerical algorithms. It is necessary to adopt the backward Euler method and derive the corresponding consistent tangent stiffness for the GLD model.

Derivation of the consistent tangent moduli becomes difficult when the constitutive equations have complicated forms. In this paper, we present a generalized approach to formulate the consistent tangent stiffness for plasticity. The derivation will be based on small-strain formulation. For finite strain plasticity, kinematic transformations are performed first so that the constitutive equations governing finite deformation

are formulated using strains–stresses and their rates defined on an *unrotated* frame of reference. Once the kinematic transformations have eliminated rotation effects on rates of the tensorial quantities, the stress updating procedure and the consistent tangent stiffness formulation remain the same as those for small-strain formulation. This treatment of the finite strain plasticity is adopted by several research and commercial finite element programs, e.g., ABAQUS. In this case, only small-strain formulation needs to be considered in development of a user material subroutine. In Section 2 we summarize the general approach to formulate the consistent tangent moduli for plasticity. The method developed in Section 2 is first applied to develop the consistent tangent stiffness for the isotropic materials with J_2 flow plasticity and the algorithm is implemented to ABAQUS via a user subroutine. The robustness and efficiency of the proposed approach are examined by comparing the performance and the analysis results with the original implementation in ABAQUS. Finally the GLD model is implemented using the proposed approach. The performance comparison between the consistent tangent stiffness and the conventional continuum tangent stiffness demonstrates the significant improvement in convergence characteristics of the overall Newton iterations caused by using the consistent tangent matrix.

2. The general method to formulate the consistent tangent matrix

In this section, a general approach to formulate the tangent moduli for plasticity, consistent with the backward Euler algorithm for the solution of the incremental problem, is presented. The algorithm is based on small-strain formulation.

2.1. The constitutive equations

Usually a yield function, a flow rule and a set of evolution equations for N state variables are needed to describe the constitutive relations of a plastic material. The yield function, Φ, for an anisotropic material can be expressed as the following general form:

$$\Phi(\sigma_{ij}, H_\alpha) = 0, \quad \alpha = 1, \ldots, N. \tag{1}$$

Here σ_{ij} are the stress components and H_α represents a set of state variables. The subscript α is introduced to indicate that there may be several state variables including the hardening parameters. When the material deforms plastically, the inelastic part of the deformation is defined by the flow rule

$$\mathrm{d}\varepsilon_{ij}^{\mathrm{p}} = \lambda \frac{\partial g}{\partial \sigma_{ij}}, \tag{2}$$

where $g = g(\sigma_{ij}, H_\alpha)$ is the plastic potential, $\mathrm{d}\varepsilon_{ij}^{\mathrm{p}}$ are the differential of the plastic strain components and λ is a positive scalar. In this study, we consider the "associated flow" plasticity model, i.e., $\Phi = g$. Finally, evolution of the N state variables can be described by

$$\mathrm{d}H_\alpha = h_\alpha(\mathrm{d}\varepsilon_{ij}^{\mathrm{p}}, \sigma_{ij}, H_\beta), \quad \alpha = 1, \ldots, N; \ \beta = 1, \ldots, N. \tag{3}$$

For complex plasticity models, several evolution equations may be defined and the forms of these equations can be very complicated. Eqs. (1)–(3) define the constitutive model for the plastic material.

2.2. Numerical integration of the plasticity model

The backward Euler method has proven to be stable and accurate for the numerical integration of the elastoplastic constitutive relations and it is especially efficient when large step size is taken. This makes it especially attractive when dealing with porous materials. Since the deformation in porous materials is

usually very large, one has to take large strain increments. Because the focus of this study is to develop the consistent tangent stiffness matrix, numerical integration of the rate constitutive equations will be described very briefly here. Detailed discussions about the backward Euler method can be found in Aravas (1987).

For the strain driven integration algorithm, which is commonly adopted in the finite element analysis, the total strain increment is known for the new increment. During the constitutive calculations, the stresses and state variables are known at the start of each increment and their values need to be updated at the end of the increment corresponding to the total strain increment. The elasticity equations give

$$(\sigma_{ij})^{t+\Delta t} = M_{ijkl}(\varepsilon^{e}_{kl})^{t+\Delta t} = M_{ijkl}\left\{(\varepsilon^{e}_{kl})^{t} + \Delta\varepsilon_{kl} - \Delta\varepsilon^{p}_{kl}\right\} = \sigma^{T}_{ij} - M_{ijkl}\Delta\varepsilon^{p}_{kl}, \tag{4}$$

where

$$\sigma^{T}_{ij} = M_{ijkl}\left\{(\varepsilon^{e}_{kl})^{t} + \Delta\varepsilon_{kl}\right\} \tag{5}$$

is the elastic predictor, t represents the time at the start of the increment, $t + \Delta t$ represents the time at the end of the increment, and the superscripts e and p denote elastic and plastic components respectively. The total strain increment $\Delta\varepsilon_{kl}$ is known, and if the linear elastic behavior is isotropic, the elastic moduli M_{ijkl} can be expressed as

$$M_{ijkl} = G(\delta_{ik}\delta_{jl} + \delta_{il}\delta_{jk}) + \left(K - \frac{2}{3}G\right)\delta_{ij}\delta_{kl}, \tag{6}$$

where G and K are the elastic shear and bulk moduli respectively, and δ_{ij} is the Kronecker delta. In Eqs. (4) and (5) and hereafter, the summation convention is used for Latin and Greek indices unless otherwise indicated.

Substituting Eq. (2) into Eq. (4) leads to

$$(\sigma_{ij})^{t+\Delta t} = \sigma^{T}_{ij} - \left(\lambda M_{ijkl}\frac{\partial \Phi}{\partial \sigma_{kl}}\right)^{t+\Delta t} \tag{7}$$

Eqs. (1), (3) and (7) consist of $N + 7$ independent equations and have $N + 7$ unknowns, i.e., six stress components, N state variables and λ. The non-linear equations can be solved iteratively by using the Newton–Raphson method.

2.3. The consistent tangent stiffness matrix

In the implicit finite element method, the equilibrium equations are written at the end of the increment, resulting a set of non-linear equations for the nodal unknowns. If a full Newton scheme is used to solve these non-linear equations, one needs to calculate the linearization moduli

$$J_{ijkl} = \left(\frac{\partial \sigma_{ij}}{\partial \varepsilon_{kl}}\right)^{t+\Delta t}. \tag{8}$$

Simo and Taylor (1985) showed that use of the consistent tangent moduli significantly improves the convergence characteristics of the overall equilibrium iterations. The so-called elastoplastic tangent derived from the "continuum" rate equations by enforcement of the consistency condition will destroy the quadratic convergence of the Newton–Raphson method. The consistent tangent stiffness corresponding to the backward Euler integration can be obtained by linearization of Eq. (4). Since all quantities in calculating J_{ijkl} are referred to time $t + \Delta t$, the superscript $t + \Delta t$ will be dropped hereafter.

Conventionally the consistent tangent stiffness matrix is obtained as follows. First, Eq. (4) can be rewritten as

$$\sigma_{ij} = M_{ijkl}\varepsilon^{e}_{kl} = M_{ijkl}(\varepsilon_{kl} - \varepsilon^{p}_{kl}) = M_{ijkl}\left\{\varepsilon_{kl} - (\varepsilon^{p}_{kl})^{t} - \Delta\varepsilon^{p}_{kl}\right\}. \tag{9}$$

Next, substitute Eq. (2) into Eq. (9) and differentiate the resulting equation

$$\partial\sigma_{ij} = M_{ijkl}\partial\varepsilon_{kl} - \partial\lambda M_{ijkl}\frac{\partial\Phi}{\partial\sigma_{kl}} - \lambda M_{ijkl}\frac{\partial^2\Phi}{\partial\sigma_{kl}\partial\sigma_{mn}}\partial\sigma_{mn}. \tag{10}$$

To obtain the tangent stiffness, $\partial\lambda$ needs to be evaluated. However, evaluation of $\partial\lambda$ becomes difficult when the derivatives of state variables (∂H_α) have complex forms in terms of $\partial\sigma_{ij}$ and $\partial\varepsilon_{ij}$. For this reason, we choose another way to derive the consistent tangent stiffness.

By directly differentiating Eq. (9), we can get

$$\partial\sigma_{ij} = M_{ijkl}\partial\varepsilon_{kl} - M_{ijkl}\partial\varepsilon^{p}_{kl}. \tag{11}$$

From the above equation, if we can find the relations between $\partial\varepsilon^{p}_{ij}$ and $\partial\sigma_{ij}$ (or $\partial\varepsilon_{ij}$), the consistent tangent stiffness matrix can be achieved. From Eq. (3) we can obtain

$$\partial H_\beta = C_{\alpha\beta}\left(\frac{\partial h_\alpha}{\partial\sigma_{ij}}\partial\sigma_{ij} + \frac{\partial h_\alpha}{\partial(\Delta\varepsilon^{p}_{ij})}\partial(\Delta\varepsilon^{p}_{ij})\right), \tag{12}$$

where $C_{\alpha\beta}$ is defined as

$$C^{-1}_{\alpha\beta} = \delta_{\alpha\beta} - \frac{\partial h_\alpha}{\partial H_\beta}. \tag{13}$$

To find the relations between $\partial\varepsilon^{p}_{ij}$ and $\partial\sigma_{ij}$, we start by taking the differentiation of the yield function

$$\mathrm{d}\Phi = \frac{\partial\Phi}{\partial\sigma_{ij}}\partial\sigma_{ij} + \frac{\partial\Phi}{\partial H_\beta}\partial H_\beta = 0. \tag{14}$$

Substituting Eq. (12) into Eq. (14) gives

$$\mathrm{d}\Phi = \frac{\partial\Phi}{\partial\sigma_{ij}}\partial\sigma_{ij} + C_{\alpha\beta}\frac{\partial\Phi}{\partial H_\beta}\frac{\partial h_\alpha}{\partial\sigma_{ij}}\partial\sigma_{ij} + C_{\alpha\beta}\frac{\partial\Phi}{\partial H_\beta}\frac{\partial h_\alpha}{\partial(\Delta\varepsilon^{p}_{ij})}\partial(\Delta\varepsilon^{p}_{ij}) = 0 \tag{15}$$

or

$$C_{\alpha\beta}\frac{\partial\Phi}{\partial H_\beta}\frac{\partial h_\alpha}{\partial(\Delta\varepsilon^{p}_{ij})}\partial(\Delta\varepsilon^{p}_{ij}) = -\left(\frac{\partial\Phi}{\partial\sigma_{ij}} + C_{\alpha\beta}\frac{\partial\Phi}{\partial H_\beta}\frac{\partial h_\alpha}{\partial\sigma_{ij}}\right)\partial\sigma_{ij}. \tag{16}$$

This gives only one equation. In order to find the relationships between the increments of stress components and the increments of the plastic strain components, eight more equations are needed.

Aravas (1987) introduced two scalar strain variables

$$\Delta\varepsilon_p = -\lambda\frac{\partial\Phi}{\partial p}, \Delta\varepsilon_q = \lambda\frac{\partial\Phi}{\partial q}$$

with p and q representing the hydrostatic stress and the equivalent stress, respectively. Eliminating λ results in

$$\Delta\varepsilon_p\left(\frac{\partial\Phi}{\partial q}\right) + \Delta\varepsilon_q\left(\frac{\partial\Phi}{\partial p}\right) = 0.$$

The two scalar strain variables introduced by Aravas have also adopted by several other authors, e.g., Lee and Zhang (1991), Zhang (1995) and Muhlich and Brocks (2003), for numerical integration of a class of pressure-dependent plasticity laws.

The same concept is employed here. The eight remaining equations needed to determine the relationships between the increments of stress components and the increments of the plastic strain components can be obtained by rearranging Eq. (2) as

$$\frac{\Delta\varepsilon_{11}^{\mathrm{p}}}{\left(\frac{\partial\Phi}{\partial\sigma_{11}}\right)}=\frac{\Delta\varepsilon_{21}^{\mathrm{p}}}{\left(\frac{\partial\Phi}{\partial\sigma_{21}}\right)}=\frac{\Delta\varepsilon_{31}^{\mathrm{p}}}{\left(\frac{\partial\Phi}{\partial\sigma_{31}}\right)}=\frac{\Delta\varepsilon_{12}^{\mathrm{p}}}{\left(\frac{\partial\Phi}{\partial\sigma_{12}}\right)}=\frac{\Delta\varepsilon_{22}^{\mathrm{p}}}{\left(\frac{\partial\Phi}{\partial\sigma_{22}}\right)}=\cdots=\frac{\Delta\varepsilon_{33}^{\mathrm{p}}}{\left(\frac{\partial\Phi}{\partial\sigma_{33}}\right)}=\lambda. \tag{17}$$

If one of the non-zero components of $\partial\Phi/\partial\sigma_{ij}$ is chosen as reference, one can obtain eight independent equations from (17). Here we assume that $\partial\Phi/\partial\sigma_{22}\neq 0$ and the eight equations resulted from Eq. (17) are as follows:

$$\begin{aligned}
\Psi_1&=\left(\frac{\partial\Phi}{\partial\sigma_{22}}\right)\Delta\varepsilon_{11}^{\mathrm{p}}-\left(\frac{\partial\Phi}{\partial\sigma_{11}}\right)\Delta\varepsilon_{22}^{\mathrm{p}}=0,\\
\Psi_2&=\left(\frac{\partial\Phi}{\partial\sigma_{22}}\right)\Delta\varepsilon_{21}^{\mathrm{p}}-\left(\frac{\partial\Phi}{\partial\sigma_{21}}\right)\Delta\varepsilon_{22}^{\mathrm{p}}=0,\\
&\vdots\\
\Psi_8&=\left(\frac{\partial\Phi}{\partial\sigma_{22}}\right)\Delta\varepsilon_{33}^{\mathrm{p}}-\left(\frac{\partial\Phi}{\partial\sigma_{33}}\right)\Delta\varepsilon_{22}^{\mathrm{p}}=0.
\end{aligned} \tag{18}$$

By differentiating equation Ψ_1 we can get

$$\begin{aligned}
\mathrm{d}\Psi_1=&\left(\frac{\partial\Phi}{\partial\sigma_{22}}\right)\partial(\Delta\varepsilon_{11}^{\mathrm{p}})+\Delta\varepsilon_{11}^{\mathrm{p}}\left(\frac{\partial^2\Phi}{\partial\sigma_{22}\partial\sigma_{ij}}\partial\sigma_{ij}+\frac{\partial^2\Phi}{\partial\sigma_{22}\partial H_\beta}\partial H_\beta\right)-\left(\frac{\partial\Phi}{\partial\sigma_{11}}\right)\partial(\Delta\varepsilon_{22}^{\mathrm{p}})\\
&-\Delta\varepsilon_{22}^{\mathrm{p}}\left(\frac{\partial^2\Phi}{\partial\sigma_{11}\partial\sigma_{ij}}\partial\sigma_{ij}+\frac{\partial^2\Phi}{\partial\sigma_{11}\partial H_\beta}\partial H_\beta\right)\\
=&\,0.
\end{aligned} \tag{19}$$

Substituting Eq. (12) into Eq. (19) and rearranging the terms result in

$$\begin{aligned}
&\left(\frac{\partial\Phi}{\partial\sigma_{22}}\right)\partial(\Delta\varepsilon_{11}^{\mathrm{p}})-\left(\frac{\partial\Phi}{\partial\sigma_{11}}\right)\partial(\Delta\varepsilon_{22}^{\mathrm{p}})+C_{\alpha\beta}\left(\Delta\varepsilon_{11}^{\mathrm{p}}\frac{\partial^2\Phi}{\partial\sigma_{22}\partial H_\beta}-\Delta\varepsilon_{22}^{\mathrm{p}}\frac{\partial^2\Phi}{\partial\sigma_{11}\partial H_\beta}\right)\frac{\partial h_\alpha}{\partial\left(\Delta\varepsilon_{ij}^{\mathrm{p}}\right)}\partial\left(\Delta\varepsilon_{ij}^{\mathrm{p}}\right)\\
&=\left(\Delta\varepsilon_{22}^{\mathrm{p}}\frac{\partial^2\Phi}{\partial\sigma_{11}\partial\sigma_{ij}}-\Delta\varepsilon_{11}^{\mathrm{p}}\frac{\partial^2\Phi}{\partial\sigma_{22}\partial\sigma_{ij}}+C_{\alpha\beta}\left(\Delta\varepsilon_{22}^{\mathrm{p}}\frac{\partial^2\Phi}{\partial\sigma_{11}\partial H_\beta}-\Delta\varepsilon_{11}^{\mathrm{p}}\frac{\partial^2\Phi}{\partial\sigma_{22}\partial H_\beta}\right)\frac{\partial h_\alpha}{\partial\sigma_{ij}}\right)\partial\sigma_{ij}.
\end{aligned} \tag{20}$$

Similarly, we can obtain the remaining seven equations by differentiating equations Ψ_2–Ψ_8. Combining the eight equations obtained above and Eq. (16), the relationships between $\partial\varepsilon_{ij}^{\mathrm{p}}$ and $\partial\sigma_{\mathrm{ij}}$ can be determined and therefore the consistent tangent stiffness can be derived from Eq. (11).

For the convenience of the finite element implementation, we will derive the consistent tangent stiffness in matrix form. The boldface symbols will be used to denote vectors and matrices. The following matrix products will be used in the equations:

$$\begin{aligned}
(\mathbf{Ad})_i&=A_{ij}d_j,\\
(\mathbf{AB})_{ij}&=A_{ik}B_{kj}.
\end{aligned}$$

The nine equations between $\partial\varepsilon_{ij}^{\mathrm{p}}$ and $\partial\sigma_{ij}$ obtained above can be summarized as

$$\mathbf{K}\partial(\Delta\varepsilon^{\mathrm{p}})=\mathbf{D}\partial\boldsymbol{\sigma}, \tag{21}$$

where $\Delta\boldsymbol{\varepsilon}^{\mathrm{p}} = \left\{\Delta\varepsilon^{\mathrm{p}}_{11}, \Delta\varepsilon^{\mathrm{p}}_{21}, \Delta\varepsilon^{\mathrm{p}}_{31}, \ldots, \Delta\varepsilon^{P}_{33}\right\}^{\mathrm{T}}$, $\boldsymbol{\sigma} = \{\sigma_{11}, \sigma_{21}, \sigma_{31}, \ldots, \sigma_{33}\}^{\mathrm{T}}$, $\mathbf{K}$ is the coefficient matrix of $\partial(\Delta\boldsymbol{\varepsilon}^{\mathrm{p}})$ and $\mathbf{D}$ is the coefficient matrix of $\partial\boldsymbol{\sigma}$. Construction of the K and D matrices are demonstrated in Section 3.

From Eqs. (21) and (11) we can obtain

$$\partial(\Delta\varepsilon^{\mathrm{p}}) = (\mathbf{K} + \mathbf{DM})^{-1}\mathbf{DM}(\partial\boldsymbol{\varepsilon}), \tag{22}$$

where $\mathbf{M}$ is a 9×9 matrix representing the elasticity tensor M_{ijkl}. Substituting Eq. (22) into Eq. (11) leads to

$$\partial\boldsymbol{\sigma} = \left(\mathbf{M} - \mathbf{M}(\mathbf{K} + \mathbf{DM})^{-1}\mathbf{DM}\right)(\partial\boldsymbol{\varepsilon}). \tag{23}$$

Therefore, the consistent tangent stiffness matrix corresponding to the backward Euler integration scheme can be obtained as

$$\mathbf{J} = \left(\frac{\partial\boldsymbol{\sigma}}{\partial\boldsymbol{\varepsilon}}\right)^{t+\Delta t} = \mathbf{M} - \mathbf{M}(\mathbf{K} + \mathbf{DM})^{-1}\mathbf{DM}. \tag{24}$$

Several comments can be made about the consistent tangent stiffness matrix derived above. (1) The procedure for deriving the consistent tangent stiffness is general and can be applied to formulate the consistent tangent stiffness matrix for plasticity models which can be described by Eqs. (1)–(3). (2) The $\mathbf{J}$ matrix is usually non-symmetric. It becomes symmetric when the material obeys the J_2 plasticity theory (Section 3). But for other plasticity models, e.g., the GLD model (see Section 4), $\mathbf{J}$ can be non-symmetric. If the deformation of the material is small, the non-symmetric contributions are insignificant compared to the symmetric contributions and a symmetric linear solver can be used to solve the structural equations. However, when the deformation becomes large, a non-symmetric solver should be used. (3) A matrix inversion operation is required to obtain the $\mathbf{J}$ matrix. For very large deformations, the matrix $\mathbf{K} + \mathbf{DM}$ could become ill-conditioned. Therefore, a robust and efficient numerical algorithm for matrix inversion should be employed. (4) The $\mathbf{J}$ matrix is derived based on all nine components of the stress and strain increments in this paper. In the actual implementation, reduced 6×6 matrices of $\mathbf{M}$, $\mathbf{K}$, $\mathbf{D}$ can be considered resulting a 6×6 $\mathbf{J}$ matrix because of the symmetries of the Cauchy stress and infinitesimal strain tensors. This reduces the computation time. (5) Evaluation of the $\mathbf{J}$ matrix becomes straightforward after matrices $\mathbf{K}$ and $\mathbf{D}$ are established. Calculation of the $\mathbf{K}$ and $\mathbf{D}$ matrices requires evaluation of the following derivatives

$$\frac{\partial\Phi}{\partial\sigma_{ij}}, \frac{\partial\Phi}{\partial H_\beta}, \frac{\partial^2\Phi}{\partial\sigma_{ij}\partial\sigma_{kl}}, \frac{\partial^2\Phi}{\partial\sigma_{ij}\partial H_\beta}, \frac{\partial h_\alpha}{\partial\sigma_{ij}}, \frac{\partial h_\alpha}{\partial\left(\Delta\varepsilon^{\mathrm{p}}_{ij}\right)}, \frac{\partial h_\alpha}{\partial H_\beta}. \tag{25}$$

3. Application to the J_2 plasticity model

To assess the algorithm developed in Section 2, we apply it to the J_2 plasticity model with isotropic hardening and compare it with the algorithm employed by ABAQUS.

3.1. Constitutive equations for J_2 plasticity

The yield function for J_2 plasticity can be expressed as

$$\Phi = \sigma_e - \bar{\sigma} = 0 \tag{26}$$

where $\sigma_e = \sqrt{(3/2)S_{ij}S_{ij}}$ is the equivalent stress, S_{ij} is the stress deviator and $\bar{\sigma}$ is the current yield stress of the material. An evolution equation can be formulated using equivalent plastic work expression as

$$\bar{\sigma}\Delta\bar{\varepsilon}^{\mathrm{p}} = \sigma_{ij}\Delta\varepsilon^{\mathrm{p}}_{ij}, \tag{27}$$

where $\Delta\bar{\varepsilon}^{\mathrm{p}}$ is the equivalent plastic strain. If the variation of the yield stress with respect to the equivalent plastic strain is defined by the hardening function as

$$\bar{h} = \frac{\Delta\bar{\sigma}}{\Delta\bar{\varepsilon}^{\mathrm{p}}}. \tag{28}$$

Eq. (27) can be rewritten as

$$\Delta\bar{\sigma} = \frac{\bar{h}\sigma_{ij}\Delta\varepsilon_{ij}^{\mathrm{p}}}{\bar{\sigma}}. \tag{29}$$

Eq. (29) has the same form as Eq. (3). Eqs. (26), (2) and (29) provide the constitutive equations for the J_2 flow plasticity theory.

3.2. Consistent tangent matrix for J_2 plasticity

Since the J_2 plasticity model has only one evolution equation, i.e., $\alpha = 1$ and $H_1 = \bar{\sigma}$, an explicit form of Eq. (12) can be obtained as

$$\partial\bar{\sigma} = \frac{\bar{h}\bar{\sigma}\Delta\varepsilon_{ij}^{\mathrm{p}}}{\bar{\sigma}^2 + \bar{h}\sigma_{mn}\Delta\varepsilon_{mn}^{\mathrm{p}}}\partial\sigma_{ij} + \frac{\bar{h}\bar{\sigma}\sigma_{ij}}{\bar{\sigma}^2 + \bar{h}\sigma_{mn}\Delta\varepsilon_{mn}^{\mathrm{p}}}\partial\left(\Delta\varepsilon_{ij}^{\mathrm{p}}\right). \tag{30}$$

By taking the differentiation of Eq. (26), we can get

$$\mathrm{d}\Phi = \frac{3}{2}\frac{S_{ij}}{\sigma_e}\partial\sigma_{ij} - \partial\bar{\sigma} = 0. \tag{31}$$

Substituting Eq. (30) into Eq. (31) leads to

$$\frac{\bar{h}\bar{\sigma}\sigma_{ij}}{\bar{\sigma}^2 + \bar{h}\sigma_{mn}\Delta\varepsilon_{mn}^{\mathrm{p}}}\partial\left(\Delta\varepsilon_{ij}^{\mathrm{p}}\right) = \left(\frac{3}{2}\frac{S_{ij}}{\sigma_e} - \frac{\bar{h}\bar{\sigma}\Delta\varepsilon_{ij}^{\mathrm{p}}}{\bar{\sigma}^2 + \bar{h}\sigma_{mn}\Delta\varepsilon_{mn}^{\mathrm{p}}}\right)\partial\sigma_{ij} \tag{32}$$

The remaining eight equations for determination of the relationships between $\partial\varepsilon_{ij}^{\mathrm{p}}$ and $\partial\sigma_{ij}$ are as follows:

$$\begin{aligned}
&\left(\frac{\partial\Phi}{\partial\sigma_{22}}\right)\partial(\Delta\varepsilon_{11}^{\mathrm{p}}) - \left(\frac{\partial\Phi}{\partial\sigma_{11}}\right)\partial(\Delta\varepsilon_{22}^{\mathrm{p}}) = \left(\Delta\varepsilon_{22}^{\mathrm{p}}\frac{\partial^2\Phi}{\partial\sigma_{11}\partial\sigma_{ij}} - \Delta\varepsilon_{11}^{\mathrm{p}}\frac{\partial^2\Phi}{\partial\sigma_{22}\partial\sigma_{ij}}\right)\partial\sigma_{ij},\\
&\left(\frac{\partial\Phi}{\partial\sigma_{22}}\right)\partial(\Delta\varepsilon_{21}^{\mathrm{p}}) - \left(\frac{\partial\Phi}{\partial\sigma_{21}}\right)\partial(\Delta\varepsilon_{22}^{\mathrm{p}}) = \left(\Delta\varepsilon_{22}^{\mathrm{p}}\frac{\partial^2\Phi}{\partial\sigma_{21}\partial\sigma_{ij}} - \Delta\varepsilon_{21}^{\mathrm{p}}\frac{\partial^2\Phi}{\partial\sigma_{22}\partial\sigma_{ij}}\right)\partial\sigma_{ij},\\
&\vdots\\
&\left(\frac{\partial\Phi}{\partial\sigma_{22}}\right)\partial(\Delta\varepsilon_{33}^{\mathrm{p}}) - \left(\frac{\partial\Phi}{\partial\sigma_{33}}\right)\partial(\Delta\varepsilon_{22}^{\mathrm{p}}) = \left(\Delta\varepsilon_{22}^{\mathrm{p}}\frac{\partial^2\Phi}{\partial\sigma_{33}\partial\sigma_{ij}} - \Delta\varepsilon_{33}^{\mathrm{p}}\frac{\partial^2\Phi}{\partial\sigma_{22}\partial\sigma_{ij}}\right)\partial\sigma_{ij}.
\end{aligned} \tag{33}$$

Here for the illustration purpose, it is assumed that $\partial\Phi/\partial\sigma_{22} \neq 0$ and the 22-component is used as reference to formulate the eight equations in Eq. (33). In the actual implementation, the reference component is chosen based on the value of $\partial\Phi/\partial\sigma_{ij}$. The ij-component will be chosen as the reference component if $\partial\Phi/\partial\sigma_{ij}$ is maximum at the integration point.

For the J_2 plasticity model

$$\begin{aligned}
&\frac{\partial\Phi}{\partial\sigma_{ij}} = \frac{3}{2}\frac{S_{ij}}{\sigma_e}\\
&\frac{\partial^2\Phi}{\partial\sigma_{ij}\partial\sigma_{mn}} = \frac{3}{2\sigma_e}\left(\delta_{im}\delta_{jn} - \frac{\delta_{ij}\delta_{mn}}{3}\right) - \frac{9}{4}\frac{S_{ij}S_{mn}}{\sigma_e^3}
\end{aligned} \tag{34}$$

and the **K** matrix in Eq. (21) can be obtained as

$$\begin{bmatrix} k_1S_{22} & 0 & 0 & 0 & -k_1S_{11} & 0 & 0 & 0 & 0 \\ 0 & k_1S_{22} & 0 & 0 & -k_1S_{21} & 0 & 0 & 0 & 0 \\ 0 & 0 & k_1S_{22} & 0 & -k_1S_{31} & 0 & 0 & 0 & 0 \\ 0 & 0 & 0 & k_1S_{22} & -k_1S_{12} & 0 & 0 & 0 & 0 \\ k_2\sigma_{11} & k_2\sigma_{21} & k_2\sigma_{31} & k_2\sigma_{12} & k_2\sigma_{22} & k_2\sigma_{32} & k_2\sigma_{13} & k_2\sigma_{23} & k_2\sigma_{33} \\ 0 & 0 & 0 & 0 & -k_1S_{32} & k_1S_{22} & 0 & 0 & 0 \\ 0 & 0 & 0 & 0 & -k_1S_{13} & 0 & k_1S_{22} & 0 & 0 \\ 0 & 0 & 0 & 0 & -k_1S_{23} & 0 & 0 & k_1S_{22} & 0 \\ 0 & 0 & 0 & 0 & -k_1S_{33} & 0 & 0 & 0 & k_1S_{22} \end{bmatrix}, \tag{35}$$

where

$$k_1 = \frac{3}{2\sigma_e}, k_2 = \frac{\bar{h}\bar{\sigma}}{\bar{\sigma}^2 + \bar{h}\sigma_{mn}.\Delta\varepsilon^{\mathrm{p}}_{mn}}. \tag{36}$$

The fifth row of the **K** matrix corresponds to Eq. (32) and the rest eight rows correspond to the equations given by Eq. (33). This arrangement ensures the diagonal elements of the **K** matrix to be non-zero. The **D** matrix can be constructed in a similar way.

It is noted that the coefficients of Eq. (32) often have much larger values than the coefficients of Eq. (33). To improve the conditions of the **K** and **D** matrices, a scaling factor is multiplied to both sides of (32), i.e., the elements in the fifth row of the **K** and **D** matrices are reduced by the same scaling factor. After the **K** and **D** matrices are established, the consistent tangent stiffness matrix **J** can be easily obtained.

We have implemented above procedure to ABAQUS via a user subroutine. We tested the algorithm by analyzing a cubic block containing a spherical hole at its center as shown in Fig. 1(a). This kind of model is often used in micromechanics study of the void growth behavior in ductile solids. Displacement boundary conditions are prescribed on the outer surfaces of the cube. The displacement components are specified on the faces of the block incrementally using the procedure developed by Faleskog et al. (1998) such that the macroscopic stress ratios remain constant during the loading history. Due to symmetry, a one-eighth symmetric model is employed, which contains 384 28-node, isoparametric, brick elements with reduced integration. Fig. 1(b) shows the deformed shape of the model. From this analysis, we found that the consistent

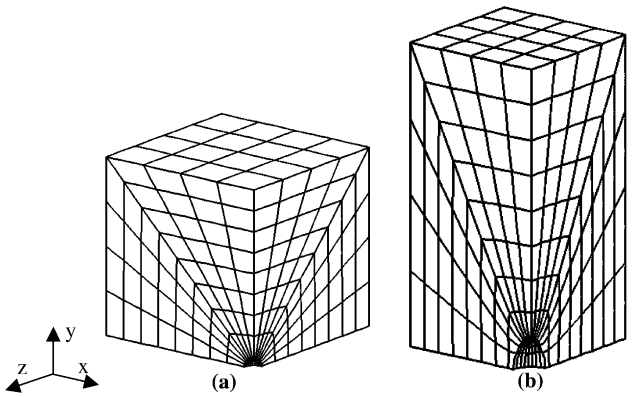

Fig. 1. (a) The one-eighth symmetric finite element mesh of a cube containing a centered spherical hole and (b) the deformed shape.

tangent stiffness matrices computed using our user subroutine are exactly the same as those computed using the algorithm originally implemented in ABAQUS during the entire loading history, which verifies our proposed method. The algorithm developed in this paper requires inverting the matrix $\mathbf{K} + \mathbf{DM}$, and therefore takes more CPU time. However, our numerical tests show that this increase of the CPU time is insignificant—it is less than 10%.

In ABAQUS the consistent tangent moduli for J_2 plasticity is derived following the conventional algorithm which requires evaluation of $\partial\lambda$. As discussed in Section 2, it is difficult to extend this approach to plasticity models with ∂H_α having complex forms in terms of $\partial\sigma_{ij}$ and $\partial\varepsilon_{ij}$. Our new approach provides a simple and efficient algorithm to formulate consistent tangent moduli for complex plasticity models.

4. Application to the GLD porous plasticity model

In this section, the algorithm developed in Section 2 is applied to derive the consistent tangent moduli for an anisotropic porous plasticity model, the GLD model, which demonstrates the effectiveness of the proposed algorithm in handling complex plasticity models.

4.1. Constitutive equations of the GLD plasticity model

The GLD porous plasticity model (Gologanu et al., 1993, 1994, 1995) provides the constitutive equations for development of the mechanism-based approaches to predict structure failure by ductile fracture (Pardoen and Hutchinson, 2000, 2003). The GLD model describes the macroscopic plastic response of ductile solids containing spheroidal voids. Because the void shape is not spherically symmetric, preferred orientations exist in the material and the plastic behavior becomes anisotropic.

Consequently, the yield function cannot be described by the stress invariants. Instead, the yield function has a complicated form involving the stress components.

Fig. 2 shows the geometrical representation of a representative material volume containing a spheroidal void (axisymmetric): (a) prolate void and (b) oblate void. The void is axisymmetric about the y-axis and the aspect ratio is $W = R_{y1}/R_{x1}$. The yield function of the void-containing material can be expressed as

$$\Phi = \frac{C}{\bar{\sigma}^2}\|\boldsymbol{\Sigma}' + \eta\Sigma_h\mathbf{X}\|^2 + 2q(g+1)(g+f)\cosh\left(\kappa\frac{\Sigma_h}{\bar{\sigma}}\right) - (g+1)^2 - q^2(g+f)^2 = 0, \tag{37}$$

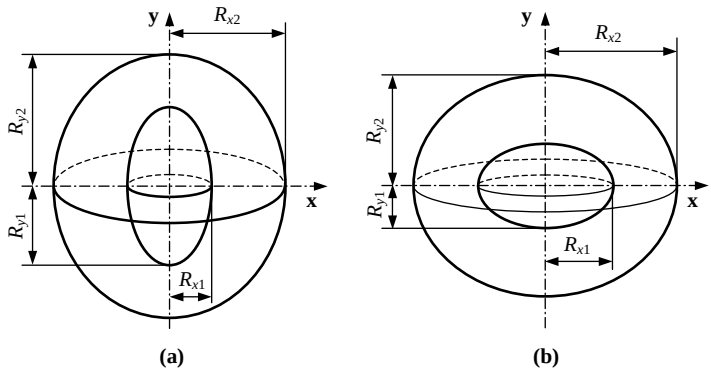

Fig. 2. Geometrical representation of a representative material volume: (a) prolate void shape and (b) oblate void shape.

where Σ_{ij} are the macroscopic stress components, f represents the void volume fraction, S is the shape parameter defined as $S = \ln(W)$, and $\bar{\sigma}$ is the yield stress of the matrix material. In Eq. (37), $\|\,\|$ denotes the von Mises norm, $\boldsymbol{\Sigma}'$ is the deviatoric stress tensor, Σ_h is the generalized hydrostatic stress defined by $\Sigma_h = \alpha_2(\Sigma_{xx} + \Sigma_{zz}) + (1-\alpha_2)\Sigma_{yy}$, $\mathbf{X}$ is a tensor defined as $\mathbf{X} = (2/3)\boldsymbol{e}_y \otimes \boldsymbol{e}_y - (1/3)\boldsymbol{e}_x \otimes \boldsymbol{e}_x - (1/3)\boldsymbol{e}_z \otimes \boldsymbol{e}_z$, where (e_x, e_y, e_z) is an orthogonal basis with $\boldsymbol{e}_y$ parallel to the axisymmetric axis of the void, and $\otimes$denotes tensor product. The parameters C, η, g, k and α_2 as described in Appendix A, are functions of f and S, and the heuristic parameter q depends on initial void volume fraction, strain hardening exponent of the matrix material, S and the macroscopic stress triaxiality factor T. Detailed descriptions about the GLD model can be found in Pardoen and Hutchinson (2000, 2003) and Gologanu et al. (2001).

In the GLD model, it is assume that the macroscopic plastic strain increments ($\Delta E^{\mathrm{p}}_{ij}$) follow the flow rule expressed as

$$\Delta E^{\mathrm{p}}_{ij} = \lambda \frac{\partial \Phi}{\partial \Sigma_{ij}} \tag{38}$$

Three evolution equations corresponding to state variables f, $\bar{\sigma}$, and S are needed in the GLD model. From the plastic incompressibility of the matrix material, the change of the void volume fraction due to void growth can be expressed as

$$\mathrm{d}f = (1-f)\mathrm{d}E^{\mathrm{p}}_{kk}. \tag{39}$$

Enforcing equality between the rates of macroscopic and matrix plastic work allows for computation of $\bar{\sigma}$ using the effective stress–strain curve for the matrix material

$$\bar{\sigma}\mathrm{d}\bar{\varepsilon}^{\mathrm{p}}(1-f) = \Sigma_{ij}\mathrm{d}E^{\mathrm{p}}_{ij}. \tag{40}$$

The evolution equation for void shape can be expressed as (Gologanu et al., 1993, 1994)

$$\mathrm{d}S = (3/2)\xi_1 \mathrm{d}E^{\mathrm{p}}_{ij} X_{ij} + \xi_2 \mathrm{d}E^{\mathrm{p}}_{kk}, \tag{41}$$

where ξ_1 and ξ_2 are described in Appendix A.

The three evolution equations can be expressed in the form of Eq. (3) as

$$\Delta f = h_1 = (1-f)\Delta E^{\mathrm{p}}_{kk}, \tag{42a}$$

$$\Delta \bar{\sigma} = h_2 = \frac{\bar{h}\Sigma_{ij}\mathrm{d}E^{\mathrm{p}}_{ij}}{\bar{\sigma}(1-f)}, \tag{42b}$$

$$\Delta S = h_3 = (3/2)\xi_1 \Delta E^{\mathrm{p}}_{ij} X_{ij} + \xi_2 \Delta E^{\mathrm{p}}_{kk} \tag{42c}$$

The rotation of the principal axis of the void is not considered here.

4.2. Consistent tangent stiffness matrix

The backward Euler method provides an accurate and stable algorithm for the numerical integration of the GLD model. But due to the complexity of the constitutive equations, it is not easy to derive the consistent tangent stiffness following the procedure by Simo and Taylor (1985). Here we use the general approach presented in Section 2 to formulate the consistent tangent stiffness matrix. The matrices $\mathbf{K}$ and $\mathbf{D}$ are needed to evaluate the consistent tangent matrix $\mathbf{J}$. To obtain these matrices, the following derivatives are required: $\frac{\partial \Phi}{\partial \Sigma_{ij}}$, $\frac{\partial \Phi}{\partial f}$, $\frac{\partial \Phi}{\partial \bar{\sigma}}$, $\frac{\partial \Phi}{\partial S}$, $\frac{\partial^2 \Phi}{\partial \Sigma_{ij}\partial \Sigma_{kl}}$, $\frac{\partial^2 \Phi}{\partial \Sigma_{ij}\partial f}$, $\frac{\partial^2 \Phi}{\partial \Sigma_{ij}\partial \bar{\sigma}}$, $\frac{\partial^2 \Phi}{\partial \Sigma_{ij}\partial S}$, $\frac{\partial h_\alpha}{\partial \Sigma_{ij}}$, $\frac{\partial h_\alpha}{\partial (\Delta E_{ij})}$, $\frac{\partial h_\alpha}{\partial f}$, $\frac{\partial h_\alpha}{\partial \bar{\sigma}}$, and $\frac{\partial h_\alpha}{\partial S}$, where $\alpha = 1, 2, 3$. These derivatives are given in Appendix B.

It is worthwhile to mention that the consistent tangent stiffness matrix **J** derived for the GLD model is non-symmetric. Therefore, a non-symmetric solver should be used for solving the structural equations, especially when deformation in the material becomes large.

4.3. Numerical tests

The numerical procedure described above has been implemented in ABAQUS via a user subroutine and tested by performing analyses of several test problems.

4.3.1. Round tensile bar

The first numerical test is conducted by analyzing necking of a round tensile bar. The 1/8-symmetric finite element mesh shown in Fig. 3(a) consists of 1122 eight-node, 3D linear brick elements hybrid with constant pressure (C3D8H in the element library of ABAQUS). A geometric imperfection is used to initiate necking at the middle of the specimen, $R_d/R_0 = 0.995$, where R_0 is the initial radius of the bar and R_d is the radius of the mid-section. The ratio of the initial length (L_0) to the initial diameter of the round bar is 4.0. Displacement boundary conditions are applied at the end of the specimen. The total axial displacement ($u_y = 0.25L_0$) is applied incrementally. The matrix material is characterized by a power-law hardening stress–strain relation with $E/\sigma_0 = 207$, $\nu = 0.3$, and $N = 0.12$, where E is the Young's modulus, σ_0 is the initial yield stress, ν is the Poisson's ratio and N is the strain-hardening exponent. The GLD model is used to describe the macroscopic plastic behavior of the material. In the first case, the voids are assumed to have a prolate shape ($W = 4$) initially and in the second case, the initial void shape is assumed to be oblate ($W = 1/4$). The initial void volume fraction for both cases is taken to be $f_0 = 0.01$.

Fig. 3(b) is the deformed shape of the tensile bar containing prolate voids showing necking occurs at the mid-section. Fig. 4 compares the engineering stress–strain curves for the two cases. Here F represents the axial load carried by the bar. The maximum load is reached at a strain value of about 0.13 (engineering strain $\varepsilon_y = u_y/L_0$). The load–elongation behavior of the bar is almost the same for both cases. The specimen containing prolate voids has a little higher ultimate strength than the specimen containing oblate voids. This kind of behavior agrees with the experimental observations by Benzerga (2000). Fig. 5 compares the radial displacements (u_r) at the mid-section of the specimen and that at the end-section of the specimen

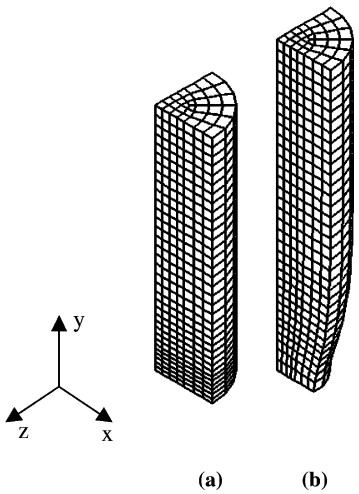

Fig. 3. (a) The 1/8-symmetric finite element mesh for analyzing necking of a round tensile bar and (b) deformed shape at $u_y = 0.25L_0$.

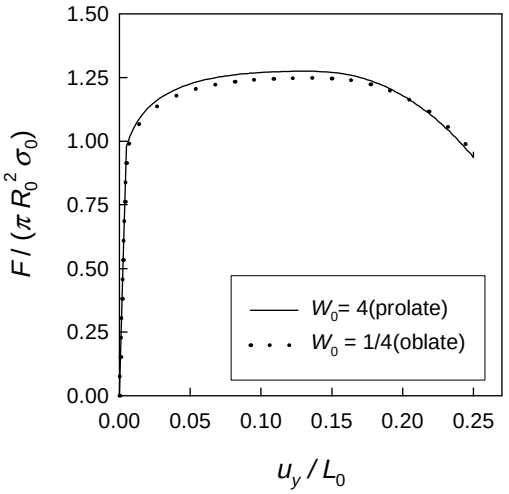

Fig. 4. Comparison of the predicted engineering stress–strain curves for specimens having prolate and oblate voids.

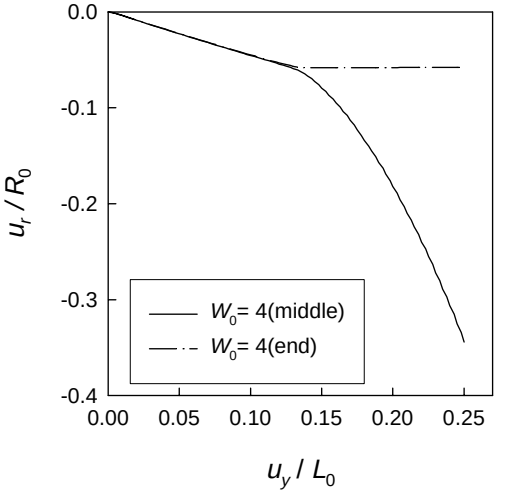

Fig. 5. Comparison of the radial contraction at the mid-section and that at the end-section of the specimen containing prolate voids.

for the prolate void case. Before u_y/L_0 reaches 0.13, uniform elongation occurs in the specimen. After u_y/L_0 reaches 0.13, the radial displacement increases rapidly around the center-length area (mid-section) of the specimen but stops changing away from the mid-section. This indicates necking of the specimen.

To demonstrate the effectiveness of the consistent tangent stiffness, the same analysis is conducted using the conventional continuum tangent moduli derived from the "continuum" rate equations by enforcement of the consistency condition. Derivation of the continuum tangent stiffness for the GLD model is straightforward (Pardoen, 2003) and the result is given in Appendix C. Fig. 6 compares the number of iterations needed to apply the same displacement increment using the consistent tangent stiffness matrix and using the continuum tangent stiffness matrix in the finite element analysis. When the deformation is small, using the consistent tangent stiffness does not lead to a noticeable reduction of the number of iterations. However,

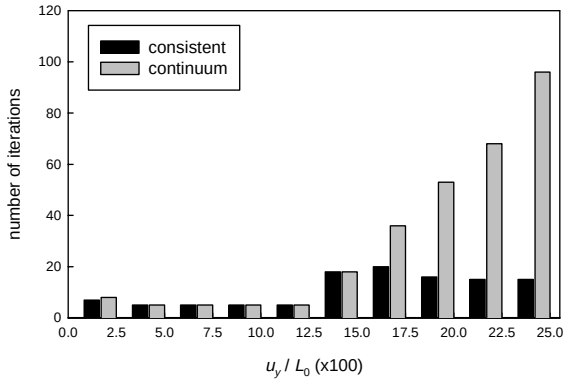

Fig. 6. Comparison of the number of iterations needed to apply the same displacement increment using the consistent tangent stiffness matrix and using the continuum tangent stiffness matrix.

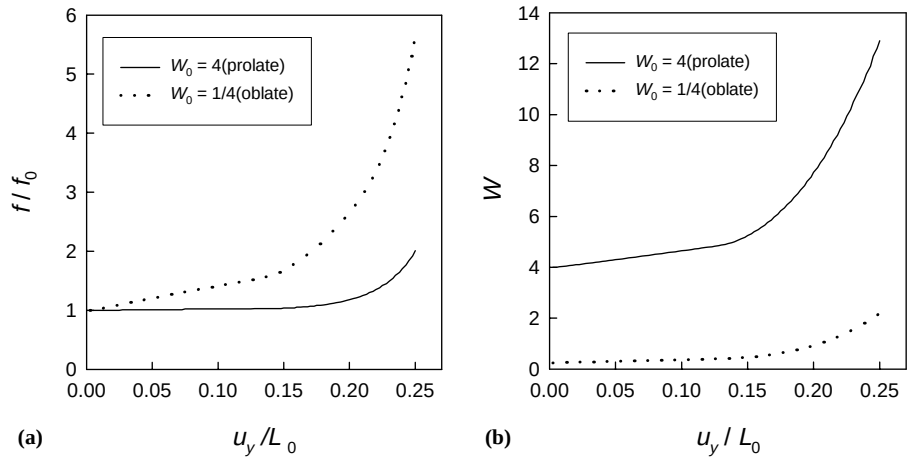

Fig. 7. Comparison of the void growth behavior of the prolate voids and the oblate voids at the center of the specimen: (a) change of void volume fraction and (b) change of void shape.

when the deformation becomes large, the advantage of using the consistent tangent stiffness is obvious. It significantly reduces the number of iterations needed to apply the same amount of displacement increment.

Although the overall load–elongation curves for the specimen containing prolate voids and the specimen containing oblate are almost the same, the void growth behavior in the two specimens is quite different. Fig. 7(a) compares the void growth rate at the center of the specimen for both cases. The oblate voids grow much faster than the prolate voids. Fig. 7(b) shows how the void aspect ratio evolves as the deformation increases. Since the load is applied in the axial direction, the initially oblate voids will change to prolate voids when $\varepsilon_y \approx 0.20$.

4.3.2. Non-uniform deformation

For the cubic material volume containing a hole considered in Section 3, the material near the hole experiences much larger deformation than the material away from the hole. To demonstrate the robustness of the consistent tangent stiffness derived for the GLD model, the finite element model shown in Fig. 1 is

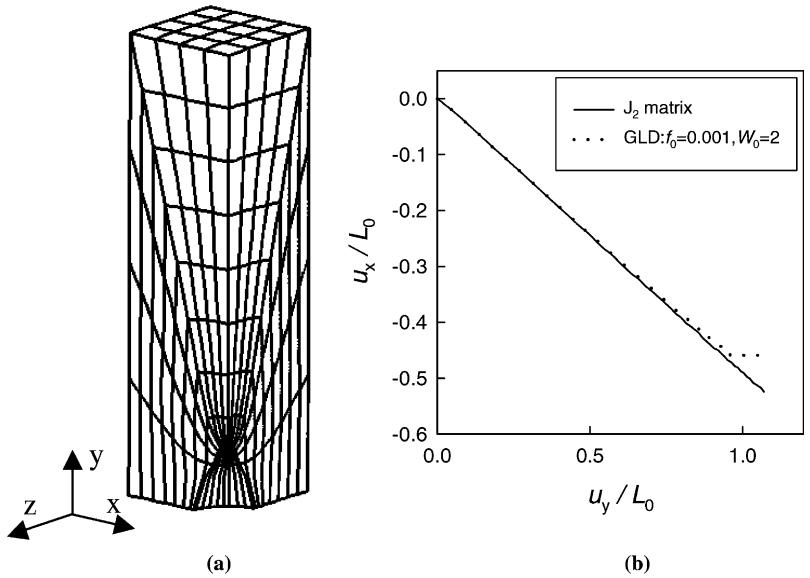

Fig. 8. (a) Deformed shape of the model and (b) comparison of the predicted variation of the lateral displacement vs. the vertical displacement curves between the J_2 material and the GLD material.

reconsidered, where length of the half-edge L_0. The boundary conditions are described in Section 3.2. Here it is assumed that the material behavior is governed by the GLD model with $f_0 = 0.001$ and $W = 2$. Fig. 8(a) shows the deformed shape of block, where the element around the hole experience very large deformation. Fig. 8(b) shows the variation of the lateral displacement (u_x) of the face perpendicular to the x-axis with the vertical displacement (u_y) of the top face. At the beginning, the block contracts laterally as the vertical displacement increases. The predicted u_x vs. u_y curves are almost the same using the J_2 plasticity model and using the GLD model. But for the GLD material, when u_y/L_0 reaches about 0.95, the lateral displacement stops changing, suggesting plastic flow localization in the ligament and onset of internal necking. This example shows that the consistent tangent stiffness derived using the proposed method has no problem dealing with non-uniform deformation and very large deformation.

5. Conclusion

In this paper, we present a general method to formulate the consistent tangent stiffness matrix for plasticity. The robustness and efficiency of the proposed approach are examined by applying it to the isotropic material with J_2 flow plasticity and comparing the performance and the analysis results with the original implementation in ABAQUS. The proposed approach is then applied to an anisotropic porous plasticity model. The performance comparison between the consistent tangent stiffness and the conventional continuum tangent stiffness demonstrates the significant improvement in convergence characteristics of the overall Newton iterations caused by using the consistent tangent matrix. Since all the stress components are used as calculation variables in the derivation of tangent stiffness matrix, the proposed method provides a general approach to formulate the consistent tangent moduli for the any plastic constitutive models given by Eqs. (1)–(3). The advantage of the proposed method becomes effective when complex plasticity models are dealt with.

Acknowledgment

This research was made possible through research funding provided by the Office of Naval Research (N00014-02-1-0423). Discussions with Prof. Pardoen of the Catholic University of Louvain (Belgium) are acknowledged.

Appendix A

The GLD model is derived from a material volume of spheroidal shape containing a confocal spheroidal void (Fig. 2). The void can be either prolate (will be referred to by the symbol "P") or oblate (will be referred to by the symbol "O"). Because of confocality, there exists a relationship $\sqrt{|R_{x1}^2 - R_{y1}^2|} = \sqrt{|R_{x2}^2 - R_{y2}^2|} = c$, where c is the focal distance. The eccentricities of the inner and outer spheroidal shapes are $e_1 = c/R_{y1}$ (P) or c/R_{x1} (O), $e_2 = c/R_{y2}$ (P) or c/R_{x2} (O). These eccentricities are related to f and S by

$$1 - e_1^2 = \exp(-2|S|), \begin{cases} f\frac{1-e_2^2}{e_2^3} = \frac{1-e_1^2}{e_1^3} & \text{(P)}, \\ f\frac{\sqrt{1-e_2^2}}{e_2^3} = \frac{\sqrt{1-e_1^2}}{e_1^3} & \text{(O)}. \end{cases} \tag{A.1}$$

The g, κ, α_2, η and C are expressed by

$$g = \begin{cases} 0 & \text{(P)}, \\ \frac{e_2^3}{\sqrt{1-e_2^2}} & \text{(O)}, \end{cases} \tag{A.2}$$

$$\kappa^{-1} = \begin{cases} \frac{1}{\sqrt{3}} + \frac{1}{\ln(f)}\left\{(\sqrt{3}-2)\ln\left(\frac{e_1}{e_2}\right) - \frac{1}{\sqrt{3}}\ln\left(\frac{3+e_1^2+2\sqrt{3+e_1^4}}{3+e_2^2+2\sqrt{3+e_2^4}}\right) + \ln\left(\frac{\sqrt{3}+\sqrt{3}+e_1^4}{\sqrt{3}+\sqrt{3}+e_2^4}\right)\right\} & \text{(P)}, \\ \frac{2}{3} + \frac{\frac{2}{3}(g_f - g_1) + \frac{2}{5}(g_f^{5/2} - g_1^{5/2}) - \left(\frac{4}{3} - g_f^{5/2} - g_1^{5/2}\right)}{\ln(g_f/g_1)}, g_f = \frac{g}{g+f}, g_1 = \frac{g}{g+1} & \text{(O)}, \end{cases} \tag{A.3}$$

$$\alpha_2 = \begin{cases} \frac{1+e_2^2}{3+e_2^4} & \text{(P)}, \\ \frac{(1-e_2^2)(1-2e_2^2)}{3-6e_2^2+4e_2^4} & \text{(O)}, \end{cases} \tag{A.4}$$

$$C = -\frac{\kappa(g+1)(g+f)\text{sh}}{\eta(Q+\eta H)}, \tag{A.5}$$

where

$$\text{sh} = \sinh(\kappa H), \quad \text{ch} = \cosh(\kappa H), \quad H = 2(\alpha_1 - \alpha_2), \quad Q = 1 - f, \tag{A.6}$$

$$\alpha_1 = \begin{cases} \frac{1}{2e_1^2} - \frac{1-e_1^2}{2e_1^3}\tanh^{-1}(e_1) & \text{(P)}, \\ -\frac{1-e_1^2}{2e_1^2} + \frac{\sqrt{1-e_1^2}}{2e_1^3}\sin^{-1}(e_1) & \text{(O)}. \end{cases} \tag{A.7}$$

The ξ_1 and ξ_2 are given by

$$\xi_1 = 1 + \frac{9}{2}\xi_T(1-\sqrt{f})\frac{\alpha_1 - \alpha_1'}{1-3\alpha_1}, \tag{A.8}$$

$$\xi_2 = \frac{1-3\alpha_1}{f} + 3\alpha_1 - 1, \tag{A.9}$$

where

$$\alpha_1' = \begin{cases} \frac{1}{3-e_1^2} & \text{(P)}, \\ \frac{1-e_1^2}{3-e_1^2} & \text{(O)}, \end{cases} \tag{A.10}$$

$$\xi_T = 1 - 0.5T, \tag{A.11}$$

$$T = \frac{(2\Sigma_{xx} + \Sigma_{yy})}{3|\Sigma_{yy} - \Sigma_{xx}|}. \tag{A.12}$$

Appendix B

Derivatives needed to formulate the consistent tangent stiffness for the GLD porous plasticity model

$$\frac{\partial \Phi}{\partial \Sigma_{ij}} = \frac{3C}{\bar{\sigma}^2}\left\{\Sigma_{kl}'\frac{\partial \Sigma_{kl}'}{\partial \Sigma_{ij}} + \eta\Sigma_h X_{kl}\frac{\partial \Sigma_{kl}'}{\partial \Sigma_{ij}} + \eta\frac{\partial \Sigma_h}{\partial \Sigma_{ij}}(\Sigma_{kl}'X_{kl} + \eta\Sigma_h X_{kl}X_{kl})\right\} + 2q(g+1)(g+f)\frac{\kappa}{\bar{\sigma}}\frac{\partial \Sigma_h}{\partial \Sigma_{ij}}\sinh\left(\kappa\frac{\Sigma_h}{\bar{\sigma}}\right), \tag{B.1}$$

$$\frac{\partial \Phi}{\partial f} = \frac{1}{\bar{\sigma}^2}\left\{\frac{\partial C}{\partial f}\frac{3}{2}(\Sigma_{ij}' + \eta\Sigma_h X_{ij})(\Sigma_{ij}' + \eta\Sigma_h X_{ij}) + 3C(\Sigma_{ij}' + \eta\Sigma_h X_{ij})\left(\frac{\partial \eta}{\partial f}\Sigma_h X_{ij} + \eta\frac{\partial \Sigma_h}{\partial f}X_{ij}\right)\right\} + 2q(g+1)(g+f)\cosh\left(\kappa\frac{\Sigma_h}{\bar{\sigma}}\right)\left\{\frac{\partial g}{\partial f}/(g+1) + \left(\frac{\partial g}{\partial f}+1\right)/(g+f)\right\} + 2q(g+1)(g+f) \times \frac{1}{\bar{\sigma}}\left(\frac{\partial \kappa}{\partial f}\Sigma_h + \kappa\frac{\partial \Sigma_h}{\partial f}\right)\sinh\left(\kappa\frac{\Sigma_h}{\bar{\sigma}}\right) - 2(g+1)\frac{\partial g}{\partial f} - 2q^2(g+f)\left(\frac{\partial g}{\partial f}+1\right), \tag{B.2}$$

$$\frac{\partial \Phi}{\partial \bar{\sigma}} = -\frac{3C}{\bar{\sigma}^3}\left\{(\Sigma_{ij}' + \eta\Sigma_h X_{ij})(\Sigma_{ij}' + \eta\Sigma_h X_{ij})\right\} - 2q(g+1)(g+f)\sinh\left(\kappa\frac{\Sigma_h}{\bar{\sigma}}\right)\kappa\frac{\Sigma_h}{\bar{\sigma}^2}, \tag{B.3}$$

$$\frac{\partial \Phi}{\partial S} = \frac{3}{2\bar{\sigma}^2}\left\{\frac{\partial C}{\partial S}(\Sigma_{ij}' + \eta\Sigma_h X_{ij})(\Sigma_{ij}' + \eta\Sigma_h X_{ij}) + 2C(\Sigma_{ij}' + \eta\Sigma_h X_{ij})\left(\frac{\partial \eta}{\partial S}\Sigma_h X_{ij} + \eta\frac{\partial \Sigma_h}{\partial S}X_{ij}\right)\right\} + 2q(g+1)(g+f)\cosh\left(\kappa\frac{\Sigma_h}{\bar{\sigma}}\right)\left\{\frac{\partial q}{\partial S}\Big/q + \frac{\partial g}{\partial S}\Big/(g+1) + \left(\frac{\partial g}{\partial f}+1\right)\Big/(g+f)\right\} + 2q(g+1)(g+f)\frac{1}{\bar{\sigma}}\left(\frac{\partial \kappa}{\partial S}\Sigma_h + \kappa\frac{\partial \Sigma_h}{\partial S}\right)\sinh\left(\kappa\frac{\Sigma_h}{\bar{\sigma}}\right) - 2(g+1)\frac{\partial g}{\partial S} - 2q\frac{\partial q}{\partial S}(g+f)^2 - 2q^2(g+f)\frac{\partial g}{\partial S}, \tag{B.4}$$

$$\frac{\partial^2 \Phi}{\partial \Sigma_{ij}\partial \Sigma_{kl}} = \frac{3C}{\bar{\sigma}^2}\left(\frac{\partial \Sigma'_{kl}}{\partial \Sigma_{ij}} + \eta X_{\mathrm{op}}\frac{\partial \Sigma_h}{\partial \Sigma_{ij}}\frac{\partial \Sigma'_{\mathrm{op}}}{\partial \Sigma_{kl}} + \eta X_{\mathrm{op}}\frac{\partial \Sigma'_{\mathrm{op}}}{\partial \Sigma_{ij}}\frac{\partial \Sigma_h}{\partial \Sigma_{kl}} + \eta\eta X_{\mathrm{op}}X_{\mathrm{op}}\frac{\partial \Sigma_h}{\partial \Sigma_{ij}}\frac{\partial \Sigma_h}{\partial \Sigma_{kl}}\right) + 2q(g+1)(g+f)\left(\frac{\kappa}{\bar{\sigma}}\right)^2\frac{\partial \Sigma_h}{\partial \Sigma_{ij}}\frac{\partial \Sigma_h}{\partial \Sigma_{kl}}\cosh\left(\kappa\frac{\Sigma_h}{\bar{\sigma}}\right), \tag{B.5}$$

$$\begin{aligned}\frac{\partial^2 \Phi}{\partial \Sigma_{ij}\partial f} = {} & \frac{3}{\bar{\sigma}^2}\frac{\partial C}{\partial f}\left\{\Sigma'_{ij} + \eta\Sigma_h X_{\mathrm{op}}\frac{\partial \Sigma'_{\mathrm{op}}}{\partial \Sigma_{ij}} + \eta\frac{\partial \Sigma_h}{\partial \Sigma_{ij}}\left(\Sigma'_{\mathrm{op}}X_{\mathrm{op}} + \eta\Sigma_h X_{\mathrm{op}}X_{\mathrm{op}}\right)\right\} \\ & + \frac{3C}{\bar{\sigma}^2}\left\{\frac{\partial \Sigma'_{\mathrm{op}}}{\partial \Sigma_{ij}}X_{\mathrm{op}}\left(\frac{\partial \eta}{\partial f}\Sigma_h + \eta\frac{\partial \Sigma_h}{\partial f}\right) + \Sigma'_{\mathrm{op}}X_{\mathrm{op}}\left(\frac{\partial \eta}{\partial f}\frac{\partial \Sigma_h}{\partial \Sigma_{ij}} + \eta\frac{\partial^2 \Sigma_h}{\partial \Sigma_{ij}\partial f}\right)\right. \\ & \left. + \eta X_{\mathrm{op}}X_{\mathrm{op}}\left(2\Sigma_h\frac{\partial \eta}{\partial f}\frac{\partial \Sigma_h}{\partial \Sigma_{ij}} + \eta\Sigma_h\frac{\partial \Sigma_h}{\partial f}\frac{\partial \Sigma_h}{\partial \Sigma_{ij}} + \eta\Sigma_h\frac{\partial^2 \Sigma_h}{\partial \Sigma_{ij}\partial f}\right)\right\} + 2q(g+1)(g+f)\frac{\kappa}{\bar{\sigma}} \\ & \times \sinh\left(\kappa\frac{\Sigma_h}{\bar{\sigma}}\right)\left[\left\{\frac{\partial g}{\partial f}\Big/(g+1) + \left(\frac{\partial g}{\partial f}+1\right) + \frac{\partial \kappa}{\partial f}\Big/\kappa\right\}\frac{\partial \Sigma_h}{\partial \Sigma_{ij}} + \frac{\partial^2 \Sigma_h}{\partial \Sigma_{ij}\partial f}\right] \\ & + 2q(g+1)(g+f)\cosh\left(\kappa\frac{\Sigma_h}{\bar{\sigma}}\right)\left(\frac{\partial \kappa}{\partial f}\Sigma_h + \kappa\frac{\partial \Sigma_h}{\partial f}\right)\frac{\kappa}{\bar{\sigma}^2}\frac{\partial \Sigma_h}{\partial \Sigma_{ij}},\end{aligned} \tag{B.6}$$

$$\begin{aligned}\frac{\partial^2 \Phi}{\partial \Sigma_{ij}\partial \bar{\sigma}} = {} & -\frac{6C}{\bar{\sigma}^3}\left\{\Sigma'_{ij} + \eta\Sigma_h X_{\mathrm{op}}\frac{\partial \Sigma'_{\mathrm{op}}}{\partial \Sigma_{ij}} + \eta\frac{\partial \Sigma_h}{\partial \Sigma_{ij}}\left(\Sigma'_{\mathrm{op}}X_{\mathrm{op}} + \eta\Sigma_h X_{\mathrm{op}}X_{\mathrm{op}}\right)\right\} - 2q(g+1)(g+f)\frac{\kappa}{\bar{\sigma}^2} \\ & \times \frac{\partial \Sigma_h}{\partial \Sigma_{ij}}\left\{\Sigma_h\frac{\kappa}{\bar{\sigma}}\cosh\left(\kappa\frac{\Sigma_h}{\bar{\sigma}}\right) + \sinh\left(\kappa\frac{\Sigma_h}{\bar{\sigma}}\right)\right\},\end{aligned} \tag{B.7}$$

$$\begin{aligned}\frac{\partial \Phi}{\partial \Sigma_{ij}\partial S} = {} & \frac{\partial C}{\partial S}\left\{\Sigma'_{ij} + \eta\Sigma_h X_{\mathrm{op}}\frac{\partial \Sigma'_{\mathrm{op}}}{\partial \Sigma_{ij}} + \eta\frac{\partial \Sigma_h}{\partial \Sigma_{ij}}\left(\Sigma'_{\mathrm{op}}X_{\mathrm{op}} + \eta\Sigma_h X_{\mathrm{op}}X_{\mathrm{op}}\right)\right\} \\ & + \frac{3C}{\bar{\sigma}^2}\left\{\frac{\partial \Sigma'_{\mathrm{op}}}{\partial \Sigma_{ij}}X_{\mathrm{op}}\left(\frac{\partial \eta}{\partial S}\Sigma_h + \eta\frac{\partial \Sigma_h}{\partial S}\right) + \Sigma'_{\mathrm{op}}X_{\mathrm{op}}\left(\frac{\partial \eta}{\partial S}\frac{\partial \Sigma_h}{\partial \Sigma_{ij}} + \eta\frac{\partial^2 \Sigma_h}{\partial \Sigma_{ij}\partial S}\right)\right. \\ & \left. + \eta X_{\mathrm{op}}X_{\mathrm{op}}\left(2\Sigma_h\frac{\partial \eta}{\partial S}\frac{\partial \Sigma_h}{\partial \Sigma_{ij}} + \eta\Sigma_h\frac{\partial \Sigma_h}{\partial S}\frac{\partial \Sigma_h}{\partial \Sigma_{ij}} + \eta\Sigma_h\frac{\partial^2 \Sigma_h}{\partial \Sigma_{ij}\partial S}\right)\right\} \\ & + 2\frac{\partial q}{\partial S}(g+1)(g+f)\frac{\kappa}{\bar{\sigma}}\sinh\left(\kappa\frac{\Sigma_h}{\bar{\sigma}}\right)\frac{\partial \Sigma_h}{\partial \Sigma_{ij}} + 2q(g+1)(g+f)\frac{\kappa}{\bar{\sigma}} \\ & \times \sinh\left(\kappa\frac{\Sigma_h}{\bar{\sigma}}\right)\left[\left\{\frac{\partial g}{\partial S}\Big/(g+1) + \left(\frac{\partial g}{\partial S}+1\right) + \frac{\partial \kappa}{\partial S}/\kappa\right\}\frac{\partial \Sigma_h}{\partial \Sigma_{ij}} + \frac{\partial^2 \Sigma_h}{\partial \Sigma_{ij}\partial S}\right] \\ & + 2q(g+1)(g+f)\cosh\left(\kappa\frac{\Sigma_h}{\bar{\sigma}}\right)\left(\frac{\partial \kappa}{\partial S}\Sigma_h + \kappa\frac{\partial \Sigma_h}{\partial S}\right)\frac{\kappa}{\bar{\sigma}^2}\frac{\partial \Sigma_h}{\partial \Sigma_{ij}}.\end{aligned} \tag{B.8}$$

Derivatives related to evolution Eqs. (42a)–(42c)

$$\begin{aligned}&\frac{\partial h_1}{\partial f} = -\Delta E^{\mathrm{p}}_{kk}, \quad \frac{\partial h_1}{\partial \bar{\sigma}} = 0, \quad \frac{\partial h_1}{\partial S} = 0, \\ &\frac{\partial h_2}{\partial f} = \frac{\bar{h}\Sigma_{ij}\Delta E^{\mathrm{p}}_{ij}}{(1-f)^2\sigma_m}, \quad \frac{\partial h_2}{\partial \bar{\sigma}} = -\frac{\bar{h}\Sigma_{ij}\Delta E^{\mathrm{p}}_{ij}}{(1-f)\sigma_m^2}, \quad \frac{\partial h_2}{\partial S} = 0, \\ &\frac{\partial h_3}{\partial f} = \frac{3}{2}\frac{\partial \xi_1}{\partial f}\Delta E^{\mathrm{p}}_{ij}X_{ij} + \frac{\partial \xi_2}{\partial f}\Delta E^{\mathrm{p}}_{kk}, \quad \frac{\partial h_3}{\partial \bar{\sigma}} = 0, \quad \frac{\partial h_3}{\partial S} = \frac{3}{2}\frac{\partial \xi_1}{\partial S}\Delta E^{\mathrm{p}}_{ij}X_{ij} + \frac{\partial \xi_2}{\partial S}\Delta E^{\mathrm{p}}_{kk},\end{aligned} \tag{B.9}$$

$$\begin{aligned}
&\frac{\partial h_1}{\partial \Sigma_{ij}} = 0, \quad \frac{\partial h_1}{\partial\left(\Delta E^{\mathrm{p}}_{ij}\right)} = (1-f)\delta_{ij},\\
&\frac{\partial h_2}{\partial \Sigma_{ij}} = \frac{\bar{h}\Delta E^{\mathrm{p}}_{kl}}{(1-f)\bar{\sigma}}\delta_{ik}\delta_{jl}, \quad \frac{\partial h_2}{\partial\left(\Delta E^{\mathrm{p}}_{ij}\right)} = \frac{\bar{h}\Sigma_{kl}}{(1-f)\bar{\sigma}}\delta_{ik}\delta_{jl},\\
&\frac{\partial h_3}{\partial \Sigma_{ij}} = \frac{3}{2}\frac{\partial \xi_1}{\partial \Sigma_{ij}}\Delta E^{\mathrm{p}}_{kl}X_{kl}, \quad \frac{\partial h_3}{\partial\left(\Delta E^{\mathrm{p}}_{ij}\right)} = \frac{3}{2}\xi_1 X_{ij} + \xi_2\delta_{ij}.
\end{aligned} \tag{B.10}$$

Appendix C

The conventional continuum tangent stiffness matrix for the GLD model

$$\mathrm{d}\sigma_{ij} = \left[M_{ijkl} - \frac{M_{ijop}M_{mnkl}\frac{\partial \Phi}{\partial \Sigma_{\mathrm{op}}}\frac{\partial \Phi}{\partial \Sigma_{mn}}}{\left\{M_{mnop}\frac{\partial \Phi}{\partial \Sigma_{mn}}\frac{\partial \Phi}{\partial \Sigma_{\mathrm{op}}} - \left(\frac{\partial \Phi}{\partial f}\frac{\partial f}{\partial \Delta\varepsilon^{\mathrm{p}}_{mn}}\frac{\partial \Phi}{\partial \Sigma_{mn}} + \frac{\partial \Phi}{\partial \bar{\sigma}}\bar{h}\frac{\partial \Phi}{\partial \Sigma_{mn}} + \frac{\partial \Phi}{\partial S}\frac{\partial S}{\partial \Delta\varepsilon^{\mathrm{p}}_{mn}}\frac{\partial \Phi}{\partial \Sigma_{mn}}\right)\right\}}\right]\mathrm{d}\varepsilon_{kl}. \tag{C.1}$$

References

ABAQUS/Theory Manual, 2001. Version 6.2, 2001. Hibbit, Karlsson and Sorensen Inc.

Aravas, N., 1987. On the numerical integration of a class of pressure-dependent plasticity models. Int. J. Numer. Methods Eng. 24, 1391–1416.

Benzerga, A.A., 2000. Rupture ductile des tôles anisotropes. Ph.D. Thesis (parts in English). Ecole des Mines de Paris.

Faleskog, J., Gao, X., Shih, C.F., 1998. Cell model for nonlinear fracture analysis—I. Micromechanics calibration. Int. J. Fract. 89, 355–373.

Gao, X., Faleskog, J., Shih, C.F., 1998a. Cell model for nonlinear fracture analysis—II. Fracture-process calibration and verification. Int. J. Fract. 89, 375–398.

Gao, X., Faleskog, J., Shih, C.F., Dodds, R.H., 1998b. Ductile tearing in part-through cracks: experiments and cell-model predictions. Eng. Fract. Mech. 59, 761–777.

Gologanu, M., Leblond, J.B., Devaux, J., 1993. Approximate models for ductile metals containing nonspherical voids—case of axisymmetric prolate ellipsoidal cavities. J. Mech. Phys. Solids 41, 1723–1754.

Gologanu, M., Leblond, J.B., Devaux, J., 1994. Approximate models for ductile metals containing nonspherical voids—case of axisymmetric oblate ellipsoidal cavities. J. Eng. Mater. Tech. 116, 290–297.

Gologanu, M., Leblond, J.B., Perrin, G., Devaux, J., 1995. Recent extensions of Gurson's model for porous ductile metals. In: Suquet, P. (Ed.), Continuum Micromechanics. Springer-Verlag, Berlin.

Gologanu, M., Leblond, J.B., Perrin, G., Devaux, J., 2001. Theoretical models for void coalescence in porous ductile solids. I. Coalescence "in layers". Int. J. Solids Struct. 38, 5581–5594.

Gurson, A.L., 1977. Continuum of ductile rupture by void nucleation and growth: part I—yield criteria and flow rules for porous ductile media. J. Eng. Mater. Tech. 99, 2–55.

Lee, J.H., Zhang, Y., 1991. On the numerical integration of a class of pressure-dependent plasticity models with mixed hardening. Int. J. Numer. Methods Eng. 32, 419–438.

Muhlich, U., Brocks, W., 2003. On the numerical integration of a class of pressure-dependent plasticity models including kinematic hardening. Comput. Mech. 31, 479–488.

Needleman, A., Tvergaard, V., 1987. An analysis of ductile rupture modes at a crack tip. J. Mech. Phys. Solids 35, 151–183.

Ortiz, M., PoPov, E.P., 1985. Accuracy and stability of integration algorithms for elastoplastic constitutive relations. Int. J. Numer. Methods Eng. 21, 1561–1576.

Pardoen, T., Hutchinson, J.W., 2000. An extended model for void growth and coalescence. J. Mech. Phys. Solids 48, 2467–2512.

Pardoen, T., Hutchinson, J.W., 2003. Micromechanics-based model for trends in toughness of ductile metals. Acta Mater. 51, 133–148.

Pardoen, T., 2003. Private communication.

Ruggieri, C., Panontin, T.L., Dodds, R.H., 1998. Numerical modeling of ductile crack growth in 3-D using computational cell elements. Int. J. Fract. 82, 95–97.

Simo, J.C., Taylor, R.L., 1985. Consistent tangent operators for rate-independent elastoplasticity. Comput. Methods Appl. Mech. Eng. 48, 101–118.

Tvergaard, V., 1982. On Localization in ductile materials containing spherical voids. Int. J. Fract. 18, 237–252.

Xia, L., Shih, C.F., Hutchinson, J.W., 1995. Computational approach to ductile crack growth under large scale yielding conditions. J. Mech. Phys. Solids 43, 389–413.

Zhang, Z.L., 1995. Explicit consistent tangent moduli with a return mapping algorithm for pressure-dependent elastoplasticity models. Comput. Methods Appl. Mech. Eng. 121, 29–44.